The Characteristics of Iris-Fed Millimeter-Wave Rectangular Microstrip Patch Antennas

MOTOHISA KANDA, SENIOR MEMBER, IEEE, DAVID C. CHANG, FELLOW, IEEE, AND DAVID H. GREENLEE

Abstract—**The fabrication of various iris-fed millimeter-wave rectangular microstrip patch antennas is described. A mathematical model is proposed to describe the iris-fed antenna. An iris having 15 percent of the area of the patch is used to couple energy into the antenna. Resonance of the antenna is observed to be insensitive to the size of the iris for irises up to 115 percent of the size of the patch. A study is also made of the coupling to the antenna as a function of position of the iris with respect to the transverse plane of the waveguide, the iris always being centered with respect to the patch. In general, the antenna has a VSWR in the waveguide feed of roughly 5:1 at resonance, except for the fully open waveguide which gives rise to a VSWR of 2.9:1 at resonance. Far-field antenna power patterns are observed to be quite broad with *H*-plane beamwidths about 130°. Maximum antenna gain observed was 4.5 dB relative to an isotropic source (dBi), with 2 dBi typical. An initial study is made of the microstrip patch antenna fed from a longitudinal waveguide wall. Results indicate that this feed structure is likely to prove valuable for microstrip patch antennas, with coupling at least as good as for the transverse-fed patch, added to the possibility of feeding multiple patches from a single waveguide.**

Key Words—**Antenna gain, aperture coupling, cavity, half-power beamwidth, iris, microstrip, millimeter wave, patch antenna, power pattern.**

Index Code—**I5d/f/j, I13d/f/j, I16d/f/j.**

I. Introduction

OVER THE PAST several years, the importance of the millimeter-wave spectrum has grown markedly. Systems requiring extremely broad-band transmission and secure communications, and a wide variety of radar applications, are responsible for the growth in utilization of these extremely high radio frequencies. To utilize this portion of the spectrum efficiently, appropriate antennas are a natural requirement. The versatility of the microstrip patch antenna at microwave frequencies suggests a potential usefulness at millimeter waves. Low cost, ease of reproduction, ruggedness, light weight, and low profile are among the advantages this class of antennas offers at any frequency, including millimeter waves.

However, it has become apparent that feed structures which operate quite well at microwave frequencies are not viable with millimeter waves. Losses become significant in microstrip lines, and coaxial feed components are not available above about 50 GHz. For this reason it is desirable to investigate a new feed for microstrip patch antennas which is useful at millimeter wavelengths, namely, the iris feed. In this structure a small hole is opened in the metallic ground plane and energy is coupled through that iris into the antenna.

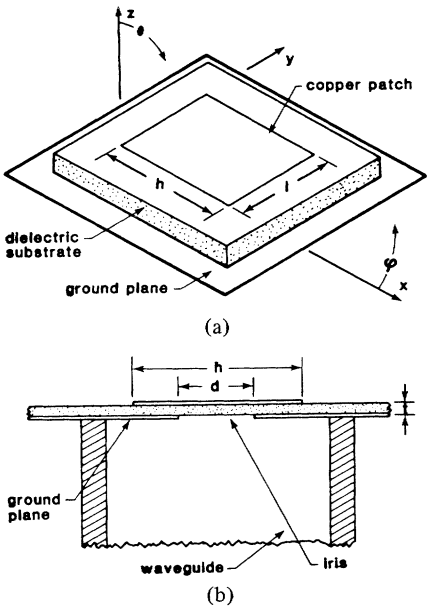

Fig. 1. (a) Rectangular microstrip patch antenna. (b) Cut-away view.

The purpose of this paper is to discuss a model relevant to the microstrip patch antenna and to present experimental results for iris-fed millimeter-wave rectangular microstrip patch antennas. Work was done at millimeter wavelengths rather than scaled to lower frequencies. This made some aspects of the work easier due to the small component sizes. However, further reductions in antenna size would have introduced severe tolerance problems in fabrication and alignment of the antennas. Also, the high frequencies made it difficult to procure the proper test equipment and sources.

II. A Model of the Iris-Fed Rectangular Microstrip Patch Antenna

A microstrip antenna is a three-layer device consisting of a dielectric substrate sandwiched between two layers of conducting material. Copper-PTFE (teflon)-copper and copper-alumina-copper sandwiches are commonly used in practice. Fig. 1 is an illustration of a rectangular microstrip patch antenna. Reference will be made throughout this paper to the dimensions and coordinate system of that drawing.

Feed effects of the microstrip patch antenna used typically

Manuscript received January 15, 1985.

M. Kanda and D. H. Greenlee are with the Electromagnetic Fields Division, National Bureau of Standards, Boulder, CO 80303. (303) 497-5320.

D. C. Chang is with the Department of Electrical Engineering, University of Colorado, Boulder, CO 80309. (303) 492-6702.

at microwave frequencies are based on a traditional coaxial probe or microstrip line feed to the antenna. The present experiment, however, was done on microstrip patch antennas with an iris feed through the ground plane. If the iris is small, there are similarities in basic assumptions and final results, particularly for the far-field pattern and dominant-mode effects. But certain parameters will be radically different for the iris-fed case, particularly the input impedance of the antenna.

One simple approach to modeling the iris-fed patch antenna is illustrated in Fig. 2. In this analysis the iris is treated as a window in the waveguide; the window is capacitive, inductive, or resonant, depending on the geometry. The feed susceptance B_f is described by a simple reactive element. For a rectangular iris centered with respect to a transverse plane of the waveguide, as in Fig. 3, the normalized susceptance B_f is given by the equation [1]

$$B_f = -(\lambda_g/a)\cot^2(\pi D/2a) + \left\{\frac{\pi(a^2-D^2)}{4aD\cos(\pi D/2a)}\right\}^2 \times \left\{\frac{(1-\lambda_0^2/4D^2)}{(1-\lambda_0^2/4a^2)}\left(\frac{4bd}{\lambda_g a}\right)\ln\csc(\pi d/2b) + (\lambda_g/aD^2)\left(\frac{b^2}{3}+\frac{d^2}{2}-\frac{8bd}{2}\right) - \left(\frac{2b^2}{\pi^2}\right)\sum_{n=1}^{\infty}(n\pi d/b)K[2n\pi(a-d)/b]/n^2\right\}$$

where

$$K(v) = \int_v^\infty dw \int_w^\infty K_0(u)\,du \cong e^{-v}(1+2v/\pi)^{-1/2}. \quad (1)$$

The admittance due to the unloaded patch is then described by the patch conductance and susceptance G_p and B_p, respectively.

A more thorough investigation, however, indicates that one cannot simply describe the iris as one susceptive element and the patch as another susceptive-conductive element acting independently. The iris will cause the excitation of higher-order modes both in the waveguide which feeds the antenna and in the cavity-like region under the patch. These modes will not be the same as those excited by an isolated identical iris in the transverse plane of a very long section of waveguide. Furthermore, the cavity behavior of a patch and substrate will be disrupted if the iris is very large, a factor not well accounted for by this model.

A more rigorous formulation of the problem is made by treating the antenna as a radiating cavity, as in the cavity and modal expansion models [2], [3], but with energy coupled into the cavity through an aperture. The antenna and feed are then modeled as in Fig. 4(a) with the sources far to the left. To represent the fields in the aperture, an equivalent magnetic current $\bar{M}_s = \bar{n} \times \bar{E}_t^a$ is assumed to be on the closed cavity wall and its negative on the closed waveguide aperture. Beginning with the following formula based on the conservation of reaction over the iris [4]

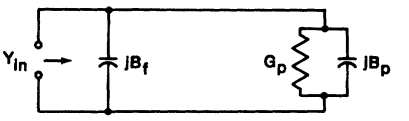

Fig. 2. Simple input-admittance model for the iris-fed patch antenna.

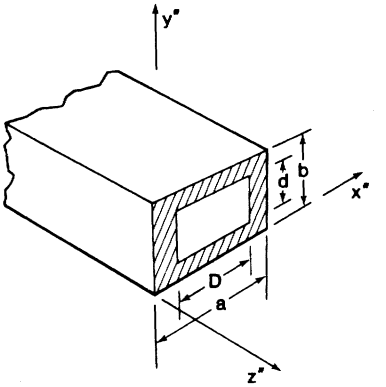

Fig. 3. Centered rectangular iris terminating a rectangular waveguide.

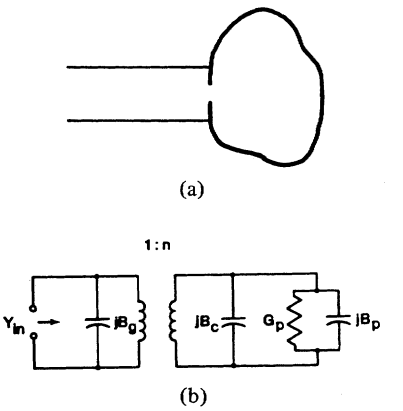

Fig. 4. (a) Aperture coupling between a rectangular waveguide and a cavity. (b) Network model of the structure.

$$\iint_A ((\bar{E}_t^a \times \bar{H}^a)\cdot \overline{ds})_{\text{guide}} = \iint_A ((\bar{E}_t^a \times \bar{H}^a)\cdot \overline{ds})_{\text{cavity}} \quad (2)$$

where the $\bar{E}_t^a$ are tangential electric fields in the aperture and the $\bar{H}^a$ are the aperture magnetic fields, it can be shown that the normalized dominant-mode admittance looking into the aperture is given by [4]

$$\frac{Y_{in}}{Y_{10}} = jB_g + \frac{n^2}{Y_{10}}\left[jB_c - j\frac{\omega(b_{10}/V)^2}{\omega^2-\omega_{10}^2}\right]. \quad (3)$$

In (3)

$$B_g = -j\sum_{mn\neq 10}\left(\frac{Y_{mn}}{Y_{10}}\frac{V_{mn}}{V_{10}}\right)^2 \quad (4)$$

is the shunt susceptance due to the waveguide side of the

aperture, and

$$B_c = -\frac{\omega}{V^2} \sum_{mn \neq 10} \frac{b_{mn}^2}{\omega^2 - \omega_{mn}^2} \tag{5}$$

is the shunt susceptance due to all higher-order cavity modes. In (5)

$$b_{mn} = \iint_A (\bar{E}_t^a \times \bar{h}_{mn}) \cdot dS \tag{6}$$

where $\bar{h}_{mn}$ are the magnetic mode vectors. For mode index mn, Y_{mn} are the characteristic wave admittances and V_{mn} the corresponding mode voltages in the waveguide. Here, $V_{10} = E_{10}(ab/2)^{1/2}$ where E_{10} is the dominant modal amplitude and ab is the waveguide cross-sectional area. By applying boundary conditions at the aperture, the related cavity voltage V and $n = V/V_{10}$ can be found. (In using (3), V need never be calculated, however, since it cancels in every term due to the normalization.)

The final term of (3) accounts for the dominant mode of the antenna. The antenna is said to be resonant when this term is purely real. However, the input susceptance of the antenna will most likely not be zero at the resonant frequency due to the susceptance of the higher-order modes, represented by B_g and B_c in Fig. 4. A discussion of the way in which the resonant frequency can be experimentally determined is presented later.

The expression for B_g was obtained from a variational solution for the susceptance of an aperture in the junction of two waveguides. That susceptance can be well approximated [4] by one-half of the susceptance of a similar aperture in a long section of the first waveguide, plus one-half of the susceptance due to the aperture in a long section of the second waveguide. Correspondingly, B_g can be approximated by one-half of the susceptance of the waveguide-antenna aperture if that aperture is located in a long section of the waveguide.

The b_{mn} terms are determined by appropriate choice of $\bar{E}_t^a$ and by using the formulas

$$\bar{h}_{mn}(x, y) = \frac{1}{j\omega\mu} [\bar{a}_x k_n \cos(k_m x) \sin(k_n y) - \bar{a}_y k_m \sin(k_m x) \cos(k_n y)]. \tag{7}$$

The resonant radian frequencies ω_{mn} are well-approximated by

$$k_{mn}^2 = \omega_{mn}^2 \mu\epsilon = k_m^2 + k_n^2 \tag{8}$$

with $k_m = m\pi/h$ and $k_n = n\pi/l$, except for the dominant mode. In that case, k_{10} must be determined.

For the radiating antenna the eigenvalues k_m and k_n are complex, with values slightly less than $m\pi/h$ and $n\pi/l$, but are closely approximated by these values for the nonradiating cavity. The one exception is k_{10}, which has a value 96–98 percent of π/h. The method by which k_{10} may be found is described as follows [2]:

$$\tan(k_{10}h) = \frac{2k_{10}\alpha_{10}}{k_{10}^2 - \alpha_{10}^2} \tag{9}$$

$$\alpha_{10} = j\frac{2\pi Z}{\lambda_0}\frac{t}{l} Y_w \tag{10}$$

where Y_w = radiating wall admittance at $x = 0, h$. The solution of (9) is found iteratively from the first two terms of a Taylor series expansion about π, that is

$$k_{10} = (\pi/h) - (\Delta_q/h) \tag{11}$$

and

$$\Delta_{p+1} = \frac{2(\alpha_{10}h)(\pi - \Delta_p)}{(\alpha_{10}h)^2 + 2\Delta_p\pi - \Delta_p^2 - \pi^2} - \frac{\Delta_p^3}{3}. \tag{12}$$

A sufficiently accurate approximation of k_{10} can usually be found by taking four iterations, that is, $q = 4$. The impedance boundary condition has little effect on the higher-order wavenumbers, which are closely approximated by $k_{mn}^2 = (m\pi/h)^2 + (n\pi/l)^2$, $mn \neq 10$.

Lacking a rigorous solution for the wall admittance, G_w is approximated to be the conductance of a TEM wave radiating into half-space from a narrow parallel-plate waveguide of width l [4]. The wall susceptance is approximated by the capacitance of an open microstrip circuit. The resulting equations for the wall admittance of the rectangular microstrip patch are

$$G_w = \frac{\pi l}{Z_0 \lambda_0} \tag{13}$$

and

$$B_w = 0.01668 \left(\frac{\Delta l}{t}\right)\left(\frac{l}{\lambda_0}\right)\epsilon_e \tag{14}$$

where

$$Z_0 = 377\ \Omega \tag{15}$$

and $\Delta l/t$ is Hammerstad's length-extension formula for a microstrip transmission line [5], and ϵ_e is Schneider's effective dielectric constant for microstrip [6]. The above two quantities are given by

$$\frac{\Delta l}{t} = 0.412 \left(\frac{\epsilon_r + 0.300}{\epsilon_r - 0.258}\right) \frac{\left(\frac{l}{t} + 0.262\right)}{\left(\frac{l}{t} + 0.813\right)} \tag{16}$$

and

$$\epsilon_e = \left(\frac{\epsilon_r + 1}{2}\right) + \left(\frac{\epsilon_r - 1}{2}\right)\left[1 + \frac{10t}{l}\right]^{-1/2}. \tag{17}$$

Further insight into the coupling mechanism of the antenna is gained by considering both the magnetic and electric dipole moments of the iris. Excitation of a z-directed E field in the cavity will be due to a magnetic dipole moment coplanar with the aperture and an electric dipole moment normal to the aperture [7]. If the aperture is very small, the guide field pattern near the aperture plane will be very close to that for a

short-circuited waveguide with field components described by

$$E_y = E_{10} \sin \frac{\pi x''}{a} \sin \frac{2\pi z''}{\lambda_g} \tag{18}$$

$$H_x = -j \frac{E_{10}}{Z_{10}} \sin \frac{\pi x''}{a} \cos \frac{2\pi z''}{\lambda_g} \tag{19}$$

and

$$H_z = j \frac{E_{10}}{Z_{10}} \frac{\lambda_g}{2a} \cos \frac{\pi x''}{a} \sin \frac{2\pi z''}{\lambda_g}. \tag{20}$$

For a very small iris, then, neither tangential electric fields nor normal magnetic fields will exist in the aperture plane. Instead, one would expect only an x-directed magnetic field.

As the iris becomes larger, both the magnetic and electric fields will have greater fringing effects. One would expect that some of the electric-field lines would bend around normal to the aperture plane and that an electric field tangent to the aperture plane would exist across the iris.

Coupling into the z-directed electric fields of the cavity by $\bar{P}_n$, the electric dipole normal to the aperture, will be small. The stronger coupling mechanism is that due to the transverse magnetic dipole $\bar{M}_t$, coplanar with the aperture. In the nearly short-circuited waveguide case, a magnetic field, or its equivalent magnetic current $\bar{J}_m$, exists in the aperture plane. The transverse magnetic dipole is proportional to $\bar{J}_m$ and codirectional with it. It is also a function of the iris geometry which determines the magnetic polarizability of the aperture. Excitation of E_z under the patch due to $\bar{M}_t$ will be maximized when $x'' = a/2$, that is, when the iris is centered with respect to the x coordinate of the waveguide opening. If the shape of the iris is given, the magnetic polarizability (a dyadic) $\bar{\bar{\alpha}}_m$ can be determined. The magnetic dipole in the aperture is then [7]

$$\bar{M}_t = \bar{\bar{\alpha}}_m \cdot \bar{H}^a. \tag{21}$$

This will be maximized, according to (19), when $x'' = a/2$.

III. The Experimental Results

Work with the microstrip patch antennas used in this project involved both the design, including choice of the antenna material, and actual fabrication. Because the dielectric constant ϵ_r of the substrate is the most critical parameter with respect to materials used, its value was selected with care. The tolerance given for the specified value of ϵ_r was of great importance since a small change in ϵ_r from the value used in the design would cause a significant error in the antenna resonant frequency as compared to the predicted value. Pertinent characteristics of these materials are presented in Table I.

Several antennas were fabricated. The iris was centered with respect to the patch in each case. Patch and iris dimensions and the size of the iris relative to the patch and relative to the waveguide cross-section area are given in Table II. The resonant frequency predicted by the transmission-line model [8] and the modal-expansion model [9], and the percentage differences between the observed and predicted values, are also presented. Finally, the normalized input impedance Z_{res} of the antenna at resonance is noted.

TABLE I
ANTENNA MATERIALS CHARACTERISTICS

Dielectric material	$\epsilon_r = 2.20 \pm 0.02$
Copper cladding density	157.5 g/m^2
thickness	71 x 10^{-6} m
tan δ	0.001
Substrate material	Random glass fiber PTFE
Thickness (t)	0.127 ± 3% mm

TABLE II
ANTENNA PARAMETERS

Antenna	No. 1	No. 2	No. 3	No. 4	No. 5
Material (ϵ_r)	2.20	2.20	2.20	2.20	2.20
Patch dimensions					
h (mm)	1.50	1.49	1.49	1.49	1.49
ℓ (mm)	1.25	1.23	1.23	1.23	1.23
Iris dimensions					
D (mm)	0.8862	0.745	0.725	0.745	0.372
d (mm)	0.862	0.392	0.372	0.392	0.725
Observed resonant frequency (GHz)	63.2	63.1	62.7	63.6	63.4
Predicted resonant frequency (trans. line) (GHz)	67.4	67.9	67.9	67.9	67.9
Error (trans. line) (%)	-6.2	-7.1	-7.7	-6.3	-6.6
Predicted resonant frequency (modal expansion)	62.4	62.8	62.8	62.8	62.8
Error (modal expansion (%)	1.3	0.5	-0.2	1.3	1.0
$\frac{\text{Iris Area}}{\text{Patch Area}}$ (%)	39.5	15.9	14.7	15.9	4.7
$\frac{\text{Iris Area}}{\text{Waveguide Area}}$ (%)	10.4	4.1	3.8	4.1	3.8
$\frac{Z_{in}}{Z_{10}}$ (at resonance)	0.23+ j0.31	0.30+ j0.40	0.15+ j0.32	0.50+ j1.37	0.87 -j0.16

The resonant frequency is defined here to be the frequency at which the final term of (3) is purely real. This corresponds to the solution of (9). Experimentally, resonance occurred at a minimum in the measured VSWR, corresponding to a minimum in the magnitude of the reflection coefficient $|\Gamma|$.

The frequency of minimum $|Y_{in}/Y_{10}|$, and consequently that of minimum $|\Gamma|$, could be determined by differentiating (3) with respect to frequency and setting that expression to zero. The dependence of (3) on ω is quite complicated and an analytical solution is difficult to find. Calculation of Y_{in}/Y_{10} for several frequencies, and from that Γ, provides an easier means

TABLE III
CALCULATED REFLECTION COEFFICIENT AND RELATED PARAMETERS FOR ANTENNA NO. 1

Frequency GHz	B_g	B_c/V^2 (S/m)x10^{-9}	$f(b_{10})$ (S/m)x10^{-8}	$\frac{1}{Y_{10}}$ (Ω)	$\frac{Y_{in}}{Y_{10}}$	Γ	$\frac{Y_{in}}{Y_{10}}'$	Γ'
60.0	-20.3	-2.18	2.63 220°	501	21.3 -86°	0.994 175°	3.37 -65°	0.793 149°
62.4	-20.2	-2.15	3.31 180°	487	20.5 -84°	0.989 174°	3.13 -44°	0.640 154°
63.2	-20.1	-2.15	3.12 163°	483	20.9 -85°	0.991 175°	3.43 -54°	0.721 153°
65.0	-19.8	-2.13	2.26 135°	474	21.0 -87°	0.996 175°	3.34 -71°	0.838 148°

of showing that the resonance does indeed correspond to a minimum in VSWR.

As an example, calculation is made of Y_{in}/Y_{10} for antenna No. 1. Dimensions of this antenna are noted in Table II. The magnetic mode vectors $\bar{h}_{mn}$ of the antenna are defined to be those of (7). The tangential aperture distribution of the electric field is approximated by

$$\bar{E}_t^a = \bar{a}_y j E_{10} \sin \frac{\pi}{D}\left(x - \frac{(h-D)}{2}\right). \tag{22}$$

The coordinate system for (22) is given in Fig. 1. Calculating the b_{mn} values up to b_{33} and finding ω_{mn} from (8) for $mn \neq 10$ results in the B_c noted in Table III. B_f is found from (1) for the given iris dimensions and B_g, as also noted in Table III, is assumed to be one-half that value. From (9), as described below, ω_{10} is found. From this and b_{10}, the final term of (3), labeled as $f(b_{10})$ in Table III, is calculated. The dominant-mode characteristic wave admittance Y_{10} of the waveguide is calculated from $Y_{10} = (1 - (f_c/f)^2)^{1/2}/Z_0$ where $Z_0 = 377$ Ω and f_c is the waveguide cutoff frequency. Finally, V_{10} is $E_{10}(ab/2)^{1/2}$ where ab is the waveguide cross-sectional area 3.78 × 1.89 mm. From this, Y_{in}/Y_{10} is calculated as well as the corresponding reflection coefficient

$$\Gamma = \frac{1 - Y_{in}/Y_{10}}{1 + Y_{in}/Y_{10}}. \tag{23}$$

These are noted in Table III. The calculated values indicate that $|\Gamma|$ does indeed have a minimum at 62.4 GHz, the resonant frequency predicted by the solution to (9).

To further illustrate the equations, $(Y_{in}/Y_{10})'$ and Γ' were calculated using a value $B_g' = B_g/10$. Maintaining the same values of the other parameters used above results in a calculated input admittance more in line with the measured values. The minimum in $|\Gamma'|$, occurring at 62.4 GHz in Table III, and the phase variation are more pronounced in this case since B_g' does not have as much effect on the calculated $(Y_{in}/Y_{10})'$ as B_g does on Y_{in}/Y_{10}.

Inspection of (3) reveals that there is more than one minimum of $|Y_{in}/Y_{10}|$. Indeed, differentiating (3) with respect to frequency, after all of the frequency-dependent effects have been included, results in an equation of fifth order in ω. Thus there are at least two, if not three, minima of $|Y_{in}/Y_{10}|$. The locations of these minima depend on the geometry of the antenna and of the waveguide feed.

Unless the phase of Y_{in}/Y_{10} has the appropriate magnitude and is rapidly varying, $|\Gamma|$ will have minima at the minima of $|Y_{in}/Y_{10}|$. It follows, then, that for the antennas studied it is reasonable to assume that the resonant frequency occurs at a frequency of minimum VSWR.

The above statement is not true in general for microstrip patch antennas. This is seen in the case where Y_{10} has approximately the same magnitude as the resonant input admittance of the antenna, and the susceptance due to the feed B_g and B_c is nonzero. Minimum VSWR will occur at some frequency where B_g and B_c tend to cancel the imaginary portion of the last term of (3), not where that term is purely real.

The calculated resonant frequency was determined from the various antenna parameters listed in Tables I and II, and using the transmission-line model [2] and the modal-expansion model [3]. This second predicted frequency is also the resonant frequency predicted by the iris-feed model.

For, example, for antenna No. 1 (with $\epsilon_r = 2.2$, $h = 150$ mm, $l = 1.25$ mm, $t = 0.127$ mm), the calculations proceeded as follows. For the transmission-line model, ϵ_r and h were needed only to obtain a predicted resonant frequency of 67.4 GHz. For the modal expansion model, Y_w was estimated to be 0.0024 + j0.00456. This was obtained by inserting the appropriate antenna parameters into (13), (14), (16), and (17). A value of λ_0 was assumed equal to 1.04 times the wavelength corresponding to the resonant frequency. Using $\Delta_0 = 0$ as a seed, (9) was solved by taking four iterations of (12). The resulting k_{10} found from (11) was $k_{10} = 1939 + j85.0$ m^{-1}, corresponding to $f_r = ck_{10}/2\pi\sqrt{\epsilon_r} = 62.4 + j2.7$ GHz. Thus the predicted resonant operating frequency of antenna No. 1, using this model, is 62.4 GHz.

In Figs. 5 and 6, the VSWR and input impedance of antenna No. 1 are plotted as a function of frequency. The input impedance, as displayed, is referenced to the ground plane of the antenna and includes the feed effects. All input-impedance plots presented here are similarly referenced to the antenna ground plane.

Inspection of Fig. 5 indicates that the resonant frequency of the antenna occurs at 63.2 GHz, the frequency of minimum VSWR of the antenna. As plotted in Fig. 6, the normalized input impedance of the antenna at resonance is $Z_{res} = 0.21 + j0.31$. The predicted input impedance (3) is $(Y_{in}/Y_{10})^{-1} = 0.0046 + j0.0476$. It is obvious that there is a large discrepancy between the predicted and the observed input

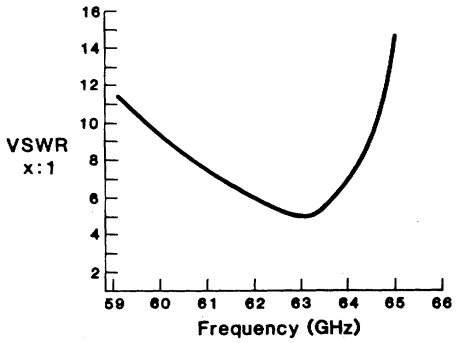

Fig. 5. VSWR versus frequency, antenna No. 1.

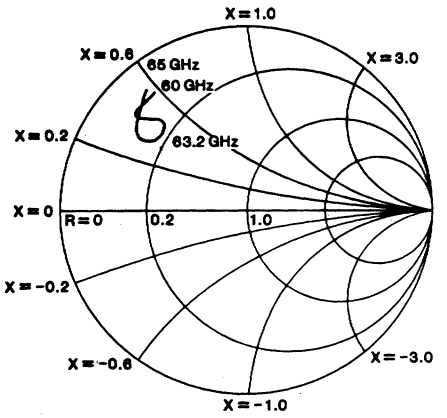

Fig. 6. Input impedance, antenna No. 1.

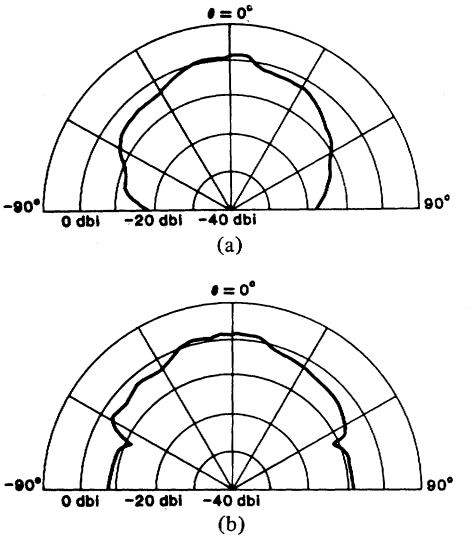

Fig. 7. Far-field power pattern, antenna No. 1, 63.2 GHz. (a) *H*-plane. (b) *E*-plane.

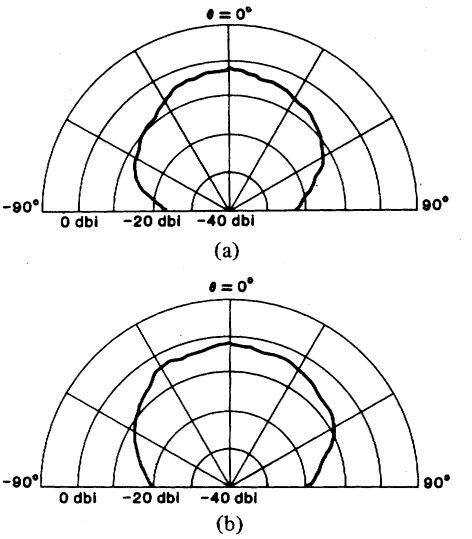

Fig. 8. *H*-plane far-field power pattern, antenna No. 1. (a) 65.4 GHz. (b) 59.2 GHz.

impedances. This is due to error in the approximation of B_g. The calculated value of B_g is much larger than that indicated by the measurements. If B_g' and $(Y_{in}/Y_{10})'$ are used instead, as noted in Table III, a more reasonable predicted input impedance of $0.23 + j0.22$ is obtained. Evidently, the model for the iris feed gives a good qualitative analysis of the problem, but fails to account completely for the susceptance introduced by the iris. A similar analysis holds for the other antennas studied.

In Fig. 7, the *H*-plane ($\phi = 0°$) and *E*-plane ($\phi = 90°$) far-field power patterns of antenna No. 1 are presented for operation at 63.2 GHz. With the standard-gain horn as a reference, the gain of antenna No. 1 was measured to be 4.0 dB relative to an isotropic source (dBi). That is, 4.0 dB greater power is received by a test antenna at the peak of the power pattern than is received from an isotropic radiator with equal transmitted power. Note that the peak power level indicated in Fig. 7 is approximately 1.3 dBi. The value 4.0 dBi is caused by the loss due to the 4.8:1 VSWR at this frequency. Throughout this paper the power patterns are drawn and scaled as they were measured, without conjugate matching. Comments in the test correlate the measured signal level with the mismatch to give the antenna gain.

The patterns of the microstrip patch antenna are fairly smooth and broad, as expected. The small undulations are assumed to be due to the effects of a finite ground plane ($5 \times 7\lambda_0$ at resonance for this antenna, and similar size for the other antennas). The *H*-plane 10-dB beamwidth is observed to be 135°, while the *E*-plane power level is down 10 dB in the $\theta = 90°$ plane. This compares to a predicted [10] 10-dB *H*-plane beamwidth of 166°. A virtually identical *H*-plane beamwidth was predicted [10] for each of the antennas No. 2–5. Yet, as will be seen, the observed beamwidths were narrower.

In Fig. 8, the *H*-plane patterns for antenna No. 1 are presented for operation at 65.4 and 59.2 GHz. The patterns are again quite broad and smooth, as at resonance, and the gain is observed to be 4.5 and 4.0 dBi, respectively. One would expect a slightly higher gain for the higher frequency case since the radiating aperture is electrically larger.

For this and all antennas tested, the polarization of the far fields was linear and in the *y* direction (Fig. 1). The cross-polarized signal level was, in general, weak enough to be entirely obscured by noise.

Antennas No. 2–4 were constructed with identical patch and nearly identical iris dimensions, as noted in Table II. Antenna

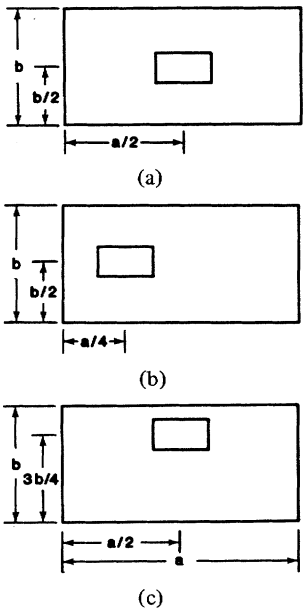

Fig. 9. Iris-waveguide orientation. (a) Antennas No. 1 and 2. (b) Antenna No. 3. (c) Antenna No. 4.

No. 2 was soldered to the waveguide section so that the iris was centered with respect to the waveguide opening, as were all of the antennas except No. 3 and 4. Antennas No. 3 and 4 were connected so that the iris was off-centered along the long axis and short axis, respectively, of the waveguide but with the iris, as always, centered with respect to the patch. This situation is illustrated in Fig. 9.

In Figs. 10 and 11, the VSWR and Smith-chart input impedance loci for antenna No. 2 are presented. It is seen from the VSWR curves that the resonance of antenna No. 2 occurs at 63.1 GHz, corresponding to an error of 0.5 percent in comparison with the predicted resonant frequency. This small discrepancy is attributable to small differences in the patch size and, secondarily, to minor variations in ϵ_r.

The *H*- and *E*-plane far-field power patterns of antenna No. 3 are shown in Fig. 12 for operation at 62.7 GHz. The signal level was low at this frequency of operation. Consequently, the peak-to-peak noise level was 2 dB at maximum received signal. This was nearly triple the noise level for all the other measurements. Even with this noise level, the pattern was discernible and is seen to be broad in both planes and similar to the patterns of antenna No. 1. The small hump in the pattern in both planes is due to the finite ground plane and, possibly, due to the antenna not being perfectly flat as mounted. The gain of antenna No. 3 at resonance is seen to be 1.5 dBi by taking into account losses due to mismatching as in Fig. 7.

The VSWR versus frequency curves and the Smith-chart input impedance loci of antennas No. 3 and 4 are presented in Figs. 13–16. Resonance is seen to occur at 62.7 and 63.6 GHz, respectively.

The normalized resonant reactance of antenna No. 3 is $j0.32$ as compared to $j0.40$ for antenna No. 2. This indicates that the feed of this antenna is more capacitive. Moving the iris in the x direction away from the center of the waveguide results in less disruption of the magnetic fields due to the iris. The result is a

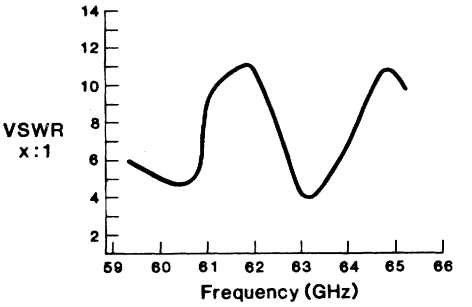

Fig. 10. VSWR versus frequency, antenna No. 2.

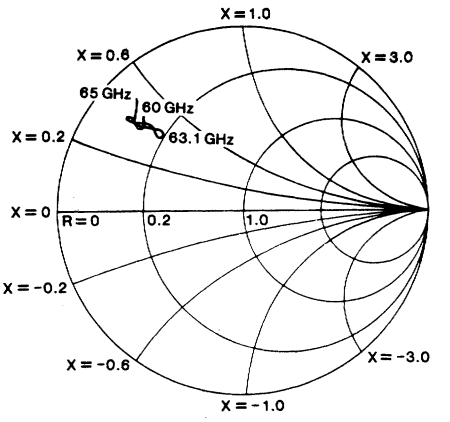

Fig. 11. Input impedance, antenna No. 2.

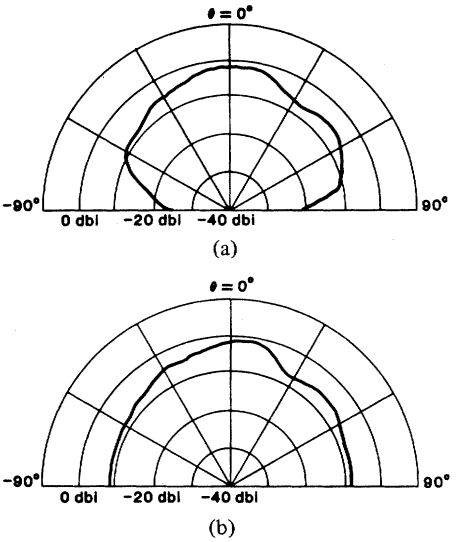

Fig. 12. Far-field power pattern, antenna No. 3, 62.7 GHz. (a) *H*-plane. (b) *E*-plane.

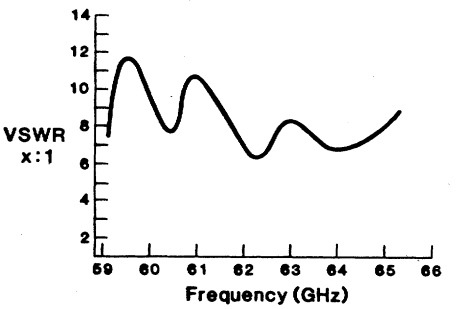

Fig. 13. VSWR versus frequency, antenna No. 4.

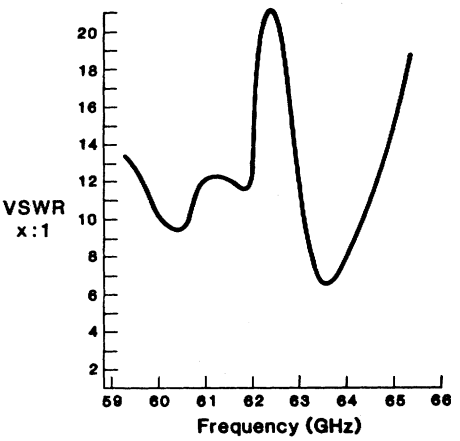

Fig. 14. VSWR versus frequency, antenna No. 5.

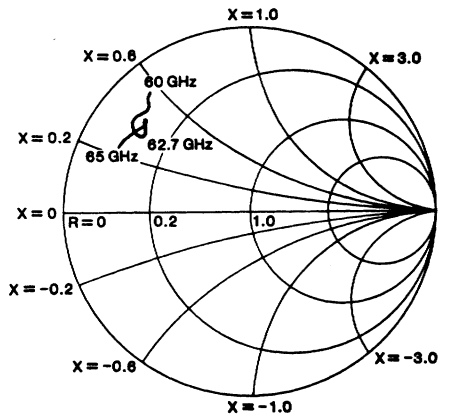

Fig. 15. Input impedance, antenna No. 4.

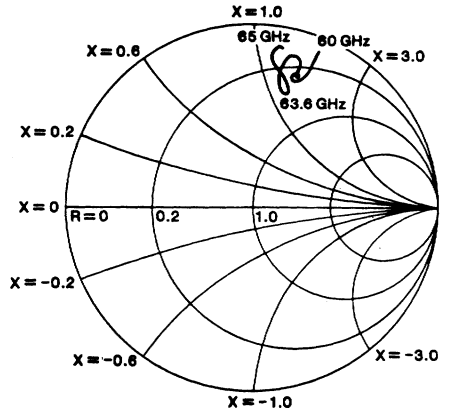

Fig. 16. Input impedance, antenna No. 5.

net reduction in stored magnetic energy, causing the antenna to be more capacitive. Moving the iris location in the x direction also reduces the transverse magnetic dipole in the aperture, decreasing the coupling into the antenna. This is seen in that the resonant VSWR is higher for this antenna than for the centered iris case.

Antenna No. 4 is seen to be much more inductive than antenna No. 2, with a resonant normalized reactance of $j1.37$. Moving the small iris in the y direction, but not the x direction, causes no change in the magnetic-field strength over the small iris in comparison to the centered case of (19). Evidently there

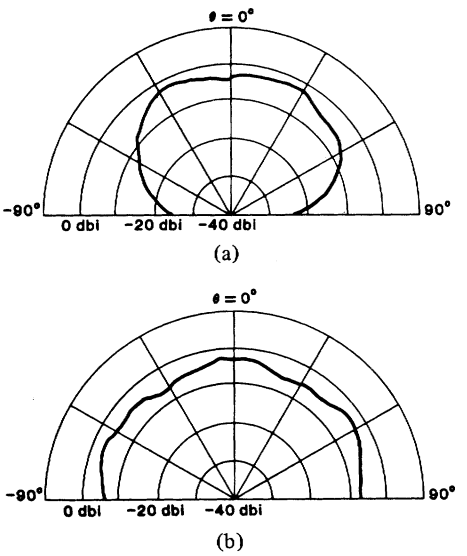

Fig. 17. Far-field power pattern, antenna No. 4, 62.7 GHz. (a) H-plane. (b) E-plane.

is a significant change in the total electric field near the aperture, with less stored electric energy for antenna No. 4 than for antenna No. 2. The mismatch of this antenna to the waveguide was very high across the whole frequency range observed. Coupling of energy into the antenna was so inefficient that the radiated signal was too small for significant far-field power pattern measurement.

In Fig. 17, the far-field H- and E-plane patterns of antenna No. 4 are presented for operation at 62.7 GHz. The patterns were similar at 63.9 GHz and at 60.5 GHz, where other minima occurred in the VSWR curve. Antenna gain at 62.7 GHz is seen to be 1.5 dBi by taking into account losses due to mismatching as in Fig. 7. The H-plane 10-dB beamwidth is observed to be 130° while the E-plane power level is down 5 dB in the $\theta = 90°$ plane. Gain at 63.9 GHz was 2.0 dBi while at 60.5 GHz it was -4 dBi, which is significantly lower (not illustrated).

An initial investigation was made into the iris-fed rectangular microstrip patch antenna fed from the longitudinal wall of the source waveguide. The patch, constructed on material with $\epsilon = 2.20$, was identical in size to the patches of antennas No. 2–4. Thus the predicted resonant frequency was 62.8 GHz according to (21). The iris, centered with respect to the patch, was of dimensions $D = 0.372$ mm and $d = 0.725$ mm.

One of the two wider walls of the WR-12 waveguide was milled away. In its place the antenna was soldered with the iris off-center 0.3 mm in the x'' direction (Fig. 3) from the center of the waveguide wall. The patch was oriented so that the y direction of the patch coincided with the z'' direction of the waveguide.

With a reflectionless termination placed after the antenna section, the input impedance of the waveguide-antenna section was measured, as plotted in Fig. 18. At the predicted resonant frequency of the antenna, 62.8 GHz, the normalized input impedance of the section was $0.87-j0.16$.

The far-field power patterns were also observed at 62.8 GHz, as illustrated in Fig. 19. The gain of the antenna, as

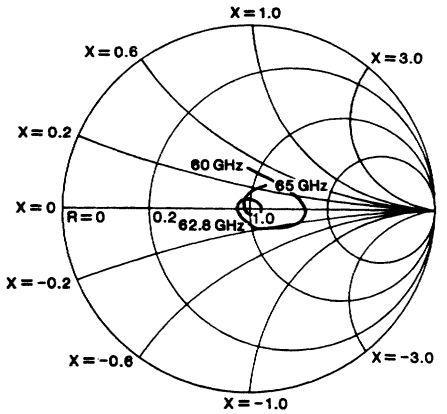

Fig. 18. Input impedance of the longitudinally fed antenna.

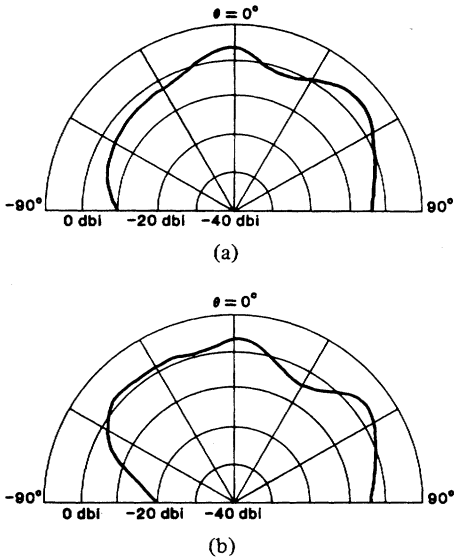

Fig. 19. Far-field power pattern, longitudinally fed antenna, 62.8 GHz. (a) *H*-plane. (b) *E*-plane.

measured by comparison with a standard gain horn, was 4.5 dBi. Undulations in the patterns are assumed to be due to reflections from the test equipment. The sharp dip in the *E*-plane pattern at $\theta = -90°$ is due to blockage from the waveguide circuit. Whereas the test equipment could be effectively screened by absorbing material below the antenna ground plane for the transverse case, such screening is not so readily accomplished for the longitudinal feed. Future work should be done using a waveguide feed circuit which is designed to eliminate such reflection problems.

The information presented here represents only preliminary results for the longitudinally fed antenna. These results do, however, indicate promise for this feed structure.

IV. Conclusion

A model was proposed to describe the iris-fed patch antenna based on aperture coupling to cavities. This model provided a good qualitative understanding of the iris-fed antenna, although the calculated input impedance did not correlate well with the measured data.

Experimental analysis was made for a variety of iris-fed patch antennas. Antennas with iris feeds of sizes ranging from 15 to 115 percent of the patch size typically exhibited a minimum VSWR in the waveguide of 5:1.

It was experimentally demonstrated that the resonant frequency of the antenna can be predicted with high accuracy by the formula related to the modal expansion model, even when the iris is 15 percent larger than the patch. This was not the case for the fully open waveguide feed.

Far-field power patterns were measured for all antennas. Maximum gain for any antenna was 4.5 dBi, with a typical value of 2 dBi. Interference between the radiation from the patch and secondary radiation from the iris feed was noted for antennas having an iris of nearly the same, or greater, size than the patch. For the fully open waveguide feed this interference was severe, except at the resonant frequency with the patch centered over the waveguide. For the smaller irises, and even for the iris slightly greater in size than the patch, the far-field patterns were quite broad with *H*-plane 10-dB beamwidths of about 130° and power level down about 10 dB in the $\theta = 90°$ plane.

It has been shown, then, that the iris feed of a microstrip patch antenna is worthy of consideration in the design of future antennas. In particular, this is true for millimeter-wave microstrip patch antennas where microstrip line and coaxial feed are impractical or unavailable.

Consideration was also given to feeding the antenna from a longitudinal waveguide wall. It is expected that more power could be coupled into the antenna by this feed structure since, with proper positioning, there would be both a tangential magnetic field over the aperture and a normal electric field. The transverse plane coupling gives rise to only tangential magnetic field over the aperture, with no normal electric field to couple into the z-directed electric fields under the patch. Initial study of this feed structure indicates that a longitudinal feed provides at least as good a coupling as that of transverse feed. Refinements in the measurements could well show this to be a superior feed structure for coupling of power into the antenna.

References

[1] L. Lewin, D. C. Chang, and E. F. Kuester, *Electromagnetic Waves and Curved Structures.* London: Peter Peregrinus, 1977.

[2] K. R. Carver and E. L. Coffey, "Theoretical investigation of the microstrip antenna," Physic. and Sci. Lab., New Mexico State Univ., Las Cruces, NM, Tech. Rep. PT-00929, Jan. 23, 1979.

[3] Y. T. Lo, D. Solomon, and W. F. Richards, "Theory and experiment on microstrip antennas," *IEEE Trans. Antennas Propagat.*, vol. AP-27, no. 2, pp. 137–145, Mar. 1979.

[4] R. F. Harrington, *Time Harmonic Electromagnetic Fields.* New York: McGraw-Hill, 1961.

[5] E. O. Hammerstad, "Equations of microstrip circuit design," in *Proc. 5th European Micro. Conf.* (Hamburg, W. Germany), Sept. 1975, pp. 268–272.

[6] M. V. Schneider, "Microstrip dispersion," *Proc. IEEE,* vol. 60, no. 1, pp. 144–146, Jan. 1972.

[7] R. E. Collin, *Field theory of Guided Waves.* New York: McGraw-Hill, 1960.

[8] S. Silver, ed., *Microwave Antenna Theory and Design.* New York: Dover, 1960.

[9] H. Jasik, ed., *Antenna Engineering Handbook.* New York: McGraw-Hill, 1961.

[10] A. G. Derneryd, "Linearly polarized microstrip antennas," *IEEE Trans. Antennas Propagat.*, vol. AP-24, no. 6, pp. 846–851, Nov. 1976.